History of Computational Pregnant Female Phantoms

Realistic computational models have been developed to simulate the morphology and internal anatomic structures of the pregnant woman at different gestational periods and were combined with Monte Carlo calculations to assess the fetal radiation dose in x-ray CT and nuclear medicine procedures (*1*). In 1995, Stabin et al. (*2*) constructed the first complete set of pregnant female models using simple mathematical surface equations. Using these mathematical models, Russell et al. (*3*) and Stabin et al. (*4*) reported estimates of the fetal dose in early pregnancy and at each trimester for a large number of radiotracers. MIRDOSE (*5*) and OLINDA/EXM (*6*), the popular personal computer software packages for internal dose assessment in nuclear medicine, also integrated this set of pregnant female models which enabled other investigators to estimate the absorbed ^{18}F-FDG dose to the fetus during different gestation periods (*7-9*). With the development of computer and tomographic imaging technologies, the construction of realistic anatomical computational models became possible (*1, 10-13*). Shi et al. (*14*) developed a tomographic pregnant female model from clinical CT images of a 30-week-pregnant patient. Later on, Xu et al. (*15*) reported a set of boundary-representation based whole-body models of pregnant females using innovative surface-geometry methods that were used in the RADAR reference phantom series for internal and external radiation dosimetry (*16*). However, most studies reported estimates of the embryo/fetal dose from ^{18}F-FDG and other positron-emitting tracers using simple mathematical pregnant female models specified in ICRP report 88 (*17*) or MIRDOSE and OLINDA/EXM packages. Since boundary-representation based models preserve much more anatomical details of organs/tissues than mathematical models, significant differences were reported between dosimetric results obtained using the two categories of models (*18-21*). With the widespread acceptance and deployment of PET/CT technology and the growth of novel and promising radiotracers targeting various molecular pathways, more accurate assessment of fetal and maternal radiation dose using new generation and more realistic anthropomorphic pregnant female phantoms according to the new ICRP 103 tissue-weighting factors (*22*) is highly desired.

The list of abbreviation (radiotracers, organs, quantities) used in this work are summarized in the Supplemental Table 1.

Organ Mass and Body Weight of Adopted Phantoms

The number of voxels in each organ was calculated and multiplied by the voxel volume and the corresponding density (*36*) to yield the organ mass. Supplemental Table 2 summarizes the organ mass, organ ID and total body weights of the voxel-based pregnant female phantoms models.

Monte Carlo Simulations

The energy deposited by photons, electrons and positrons in the target regions was recorded in unit of MeV per particle and used for the calculation of S-values from positron-emitting radionuclides. The decay data of the investigated radionuclides were obtained from the Health Physics Society electronic resource (*38*). The elemental compositions of tissue were obtained from ICRP 89 (*36*). A total of 1.0×10^{7} primary particle histories were generated such that the statistical uncertainty in terms of coefficient of variation (COV) was less than 2% in most cases. The MCPLIB02 data library for photon transport and electron-physics models was adopted for simulations performed on a workstation with 2.4 GHz Intel Xeon processors running under Microsoft Windows 7 operating system.

Radiotracers

Potential clinical applications and sources of the biodistribution data of the various radiotracers used in this work are listed in Supplemental Table 3.

Dosimetric Calculations

In the Medical Internal Radiation Dose (MIRD) formalism, the radiation absorbed dose delivered to any target tissue r_T from source organ r_S is given by Supplemental Eq. 1 and Supplemental Eq. 2 (*43*):

$$D\left(r_T, T_D\right) = \sum_{r_S} \tilde{A}(r_S, T_D) S(r_T \leftarrow r_S), \qquad \text{Supplemental Eq. 1}$$

$$S(r_T \leftarrow r_S) = \frac{1}{M(r_T)} \sum_i E_i Y_i \phi(r_T \leftarrow r_S, E_i), \qquad \text{Supplemental Eq. 2}$$

where $\tilde{A}(r_S, T_D)$ is the cumulated activity in the source organ over the dose-integration

period T_D, $S(r_T \leftarrow r_S)$ is the S-value describing the equivalent dose rate in the target organ per unit activity in the source organ, E_i is the individual energy of the ith radiation, Y_i is the yield of ith radiation per nuclear transformation and $M(r_T)$ is the mass of the target tissue. $\phi(r_T \leftarrow r_S, E_i)$ is the absorbed fraction given by E_d / E_i, where E_d refers to the deposited energy in the target tissue of the ith radiation emitted from source.

To relate the absorbed dose to stochastic effects and assess the combined detriment from stochastic effects in all organs/tissues of the human body, the concept of the effective dose was adopted by the ICRP (*34*), and is defined as:

$$E = \sum_T \omega_T \sum_R \omega_R D_R (r_T, T_D), \qquad \text{Supplemental Eq. 3}$$

where E is the effective dose, ω_T is the tissue weighting factor for organ/tissue T reflecting its relative radiation sensitivity, ω_R is the radiation weighting factor for radiation type R reflecting the linear energy transfer of the radiation, and $D_R(r_T, T_D)$ is the contribution of radiation type R to the total absorbed dose. The values of ω_R and ω_T given by the ICRP Publication 103 (*34*) were utilized to calculate the effective dose.

The effective dose was calculated by using the weighting factors listed in Supplemental Table 4. The weighting factors of bone marrow and bone surface were applied to skeleton. The tissue waiting factors of organs not in the absorbed dose list were apportioned to adrenals, gallbladder wall, heart wall, kidneys, remainder, pancreas, SI wall and cont., spleen, thymus and uterine wall of the considered pregnant phantoms.

Cross-absorbed S-values for The Fetus

Supplemental Figure 1 shows the cross-absorbed S-values of the fetus from the UB and maternal body. For all positron-emitting radionuclides, the cross-absorbed S-values decrease while the fetal weight increases. The average relative difference of S-values per Kg difference in fetal weight (%/Kg) for the UB and maternal body irradiating the fetus of the considered radionuclides between the 3-mo and the 9-mo pregnant female models are -23.8%/Kg and -12.1%/Kg, respectively. Overall, for all considered radionuclides, Cu-64 produces the smallest

self-absorbed and cross-absorbed S-values for the fetus because of its high yield of low-energy Auger electrons. Rb-82 and Y-86 produce the largest self-absorbed and the largest cross-absorbed S-values in the fetus, respectively.

Relative Contributions of Particles to Fetal S-values

The energy deposition in each target region from electrons, positrons, annihilation photons, and other photons and x-rays were recorded in particle transport simulations. Supplemental Figure 2 shows the relative contributions of electrons, positrons, the two annihilation photons and other photons and x-rays to the S-values of the fetus and maternal body irradiating the fetus for the 9 considered radionuclides. For most radionuclides, except Cu-64 and Y-86, the larger contribution (more than 55%) to the self-absorbed fetal S-values is due to positron interactions. The cross-absorbed fetal S-values of C-11, F-18, Rb-82, Ga-68, N-13, O-15 and Cu-64 are mostly (> 68%) contributed by the 511 keV annihilation photons, while the cross-absorbed fetal S-values of Y-86 and I-124 are mostly (> 75%) contributed by other photons and x-rays. Supplemental Figure 2 compares the contributions of different types of radiation emitted by Ga-68 and I-124 to the fetal S-values between different gestations when the source is in the fetus or the maternal body. It was observed that when the fetal weight and age increase, the contribution of positrons and photons to fetal S-values decrease and increase, respectively.

References:

1. Zaidi H, Xu XG. Computational anthropomorphic models of the human anatomy: The path to realistic Monte Carlo modeling in medical imaging. *Annu Rev Biomed Eng.* 2007;9(1):471-500.

2. Stabin MG. *Mathematical models and specific absorbed fractions of photon energy in the nonpregnant adult females and at the end of each trimester of pregnancy.* Oak Ridge, TN: Oak Ridge National Laboratory; 1995. ORNMM-12907.

3. Russell JR, Stabin MG, Sparks RB, Watson E. Radiation absorbed dose to the embryo/fetus from radiopharmaceuticals. *Health Phys.* 1997;73(5):756-769.

4. Stabin MG. Proposed addendum to previously published fetal dose estimate tables for 18F-FDG. *J Nucl Med.* Apr 2004;45(4):634-635.

5. Stabin MG. MIRDOSE: personal computer software for internal dose assessment in nuclear medicine. *J Nucl Med.* Mar 1996;37(3):538-546.

6. Stabin MG, Sparks RB, Crowe E. OLINDA/EXM: The second-generation personal computer software for internal dose assessment in nuclear medicine. *J Nucl Med.* June 1, 2005 2005;46(6):1023-1027.

7. Zanotti-Fregonara P, Jan S, Champion C, et al. In vivo quantification of 18F-FDG uptake in human placenta during early pregnancy. *Health Phys.* Jul 2009;97(1):82-85.

8. Zanotti-Fregonara P, Jan S, Taieb D, et al. Absorbed 18F-FDG dose to the fetus during early pregnancy. *J Nucl Med.* May 2010;51(5):803-805.

9. Takalkar AM, Khandelwal A, Lokitz S, Lilien DL, Stabin MG. 18F-FDG PET in pregnancy and fetal radiation dose estimates. *J Nucl Med.* Jul 2011;52(7):1035-1040.

10. Li A, Liu Q, Zeng S, Tang L, Zhong S, Luo Q. Construction and visualization of high-resolution three-dimensional anatomical structure datasets for Chinese digital human. *Chinese Science Bulletin.* 2008;53(12):1848-1854.

11. Zhang G, Xie T, Bosmans H, Liu Q. Development of a rat computational phantom using boundary representation method for Monte Carlo simulation in radiological imaging. *Proceedings of the IEEE.* 2009;97(12):2006-2014.

12. Xie T, Bolch WE, Lee C, Zaidi H. Pediatric radiation dosimetry for positron-emitting radionuclides using anthropomorphic phantoms. *Medical Physics.* 2013;40(10):102502.

13. Xie T, Zaidi H. Evaluation of radiation dose to anthropomorphic paediatric models from positron-emitting labelled tracers. *Physics in Medicine and Biology.* 2014;59(5):1165.

14. Shi CY, Xu XG. Development of a 30-week-pregnant female tomographic model from computed tomography (CT) images for Monte Carlo organ dose calculations. *Med Phys.* 2004;31(9):2491-2497.

15. Xu XG, Taranenko V, Zhang J, Shi C. A boundary-representation method for designing whole-body radiation dosimetry models: pregnant females at the ends of three gestational periods—RPI-P3, -P6 and -P9. *Phys Med Biol.* 2007;52(23):7023-7044.

16. Stabin MG, Xu XG, Emmons MA, Segars WP, Shi C, Fernald MJ. RADAR reference adult, pediatric, and pregnant female phantom series for internal and external dosimetry. *J Nucl Med.* 2012;53(11):1807-1813.

17. ICRP. publication 88: Doses to the embryo and fetus from intakes of radionuclides by the mother. *Ann ICRP.* 2001;31(1-3):19-515.

18. Xie T, Zaidi H. Assessment of S-values in stylized and voxel-based rat models for positron-emitting radionuclides. *Mol Imaging Biol.* 2013;15(5):542-551.

19. Xie T, Zhang G, Li Y, Liu Q. Comparison of absorbed fractions of electrons and photons using three kinds of computational phantoms of rat. *Appl Phys Lett.* Jul 19 2010;97(3):33702-33704.

20. Kramer R, Khoury H, Vieira J. Comparison between effective doses for voxel-based and stylized exposure models from photon and electron irradiation. *Physics in Medicine and Biology.* 2005;50(21):5105.

21. Lee C, Lee C, Bolch WE. Age-dependent organ and effective dose coefficients for external photons: a comparison of stylized and voxel-based paediatric phantoms. *Physics in Medicine and Biology.* 2006;51(18):4663.

22. ICRP. publication 103: The 2007 Recommendations of the International Commission on Radiological Protection. *Ann ICRP.* 2007;37(2-4):1-332.

Supplemental Table 1. List of abbreviations used in this work.

Acronyms	
GB	Gall Bladder
SI	Small Intestine
LI	Large Intestine
UB	Urinary Bladder
TB	Total Body
[11]C-SA4503	^{11}C-1-(3,4-dimethoxyphenethyl)-4-(3-phenylprophyl)piperazine
[11]C-MPDX	^{11}C-8-dicyclopropylmethyl-1-methyl-3-propylxanthine
[11]C-TMSX	[11]C-(*E*)-8-(3,4,5-trimethoxystyryl)-1,3,7-trimethylxanthine
[11]C-CHIBA-1001	4-^{11}C-methylphenyl 1,4-diazabicyclo[3.2.2.]nonane-4-carboxylate
[11]C-4DST	[11]C-4'-thiothymidine
^{18}F-FDG	2-[^{18}F]Fluoro-2-deoxy-D-glucose
[18]F-L-dopa	6-[^{18}F]Fluoro-L-dopa
^{18}F-FBPA	4-borono-2-^{18}F-fluoro-L-phenylalanine
^{18}F-FDOPA	6-[^{18}F]Fluorodopamine
^{68}Ga-EDTA	^{68}Ga-ethylenediaminetetraacetic acid
^{68}Ga-DOTANOC	[68]Ga-[1,4,7,10-Tetraazacyclododecane-1,4,7,10-tetraacetic acid]-1-Nal[3]-octreotide
ICRP	International Commission on Radiological Protection
EANM	European Association of Nuclear Medicine
PCC	phaeochromocytoma

Supplemental Table 2. Organ masses, organ ID and total body weights of the pregnant female phantoms.

Organ mass (g)	Organ ID	Early pregnancy	Gestation		
			3 month	6 month	9 month
Adrenals	11	13.0	13.1	13.1	13.1
UB	112	240.0	168.5	146.7	82.2
UB wall	12	40.0	40.0	40.0	40.0
UB cont.	13	200.0	128.5	106.7	42.2
Brain	14	1300.0	1313.6	1313.6	1313.6
Breasts	15	500.1	531.7	741.6	841.2
Esophagus	16	35.0	34.7	34.7	34.7
Eyeballs	17	14.6	15.1	15.0	15.0
Eye lens	18	0.4	0.4	0.4	0.4
GB	119	56.0	56.3	56.3	56.3
GB wall	19	10.3	8.0	8.0	8.0
GB cont.	20	45.8	48.3	48.3	48.3
Heart	121	620.0	625.5	625.5	625.5
Heart wall	21	250.0	254.9	254.9	255.5
Heart cont.	22	370.0	370.6	370.6	369.9
Kidneys	23	275.2	276.1	276.1	276.1
LI	124	679.6	683.0	679.9	677.3
LI wall	24	360.0	361.8	359.9	358.6
LI cont.	25	319.6	321.2	320.0	318.7
Liver	26	1400.0	1399.6	1399.6	1399.6
Lungs	27	950.0	950.1	950.1	950.1
Ovaries	28	11.1	11.0	11.0	11.0
Pancreas	29	120.1	119.7	119.8	119.7
SI wall and cont.	30	880.0	881.2	879.9	881.3
Skeleton	31	7760.1	7797.5	7797.5	7798.2
Skin	32	2300.8	2355.7	2487.5	2623.4
Spleen	33	130.1	128.0	128.0	128.0
Stomach	134	370.0	368.5	370.4	370.4
Stomach wall	34	140.0	138.8	139.1	139.1
Stomach cont.	35	230.0	229.7	231.4	231.4
Thymus	36	20.0	20.3	20.3	20.3
Thyroid	37	17.0	16.9	16.9	16.9
Trachea	38	8.0	8.0	8.0	8.0
Uterine wall	39	80.0	265.8	539.8	1025.5
Uterine cont.	40	-	859.6	3655.0	4113.8
Placenta	41	-	47.1	319.1	649.4
Remainder	10	42236.9	43895.3	44433.2	46615.7

TB-Fetus	200	-	85.0	1115.0	3495.0
Fetal soft tissue	42	-	71.3	903.6	2754.4
Fetal brain	43	-	13.7	133.1	371.2
Fetal skeleton	44	-	0.0	78.3	369.4
Total Body (kg)	100	60.0	62.9	68.2	74.2

Xie and Zaidi

Supplemental Table 3. List of considered compounds, applications and references of adopted biokinetic data.

| Radiotracer	Applications	References for biokinetic data
[11]C-Acetate	Myocardial oxidative metabolism and pancreatic or prostate disease	ICRP 106 (*48*)
[11]C-Amino acids	Protein synthesis	ICRP 106 (*48*)
[11]C-Brain receptor substances	Molecular imaging of different cerebral receptors	ICRP 106 (*48*)
[11]C-Methionine	Protein synthesis	ICRP 106 (*48*)
[11]C(Realistic maximum model)	Realistic maximum model for ^{11}C labeled radiotracers	ICRP 106 (*48*)
[Methyl-^{11}C]-Thymidine	Cell proliferation in malignant tumors	ICRP 80 (*49*)
[11]C-Thymidine	Cell proliferation in malignant tumors	ICRP 80 (*49*)
[11]C-SA4503	Sigma1 receptor	Sakata et al. (*39*)
[11]C-MPDX	Adenosine A1 receptor	Sakata et al. (*39*)
[11]C-TMSX	Adenosine A2A receptor	Sakata et al. (*39*)
[11]C-CHIBA-1001	DNA synthesis	Sakata et al. (*39*)
[11]C-4DST	DNA synthesis	Sakata et al. (*39*)
[15]O-water	Blood flow measurement	ICRP 80 (*49*)
[18]F-Amino acids	Protein synthesis	ICRP 106 (*48*)
[18]F-Brain receptor substances	Molecular imaging of different cerebral receptors	ICRP 106 (*48*)
^{18}F-FDG	Glucose metabolism	ICRP 106 (*48*)
[18]F-L-dopa	Dopamine metabolism and dopaminergic function	ICRP 106 (*48*)
^{18}F-FBPA	Effect prediction of boron neutron capture therapy	Sakata et al. (*39*)
^{18}F-FDOPA	Imaging of sympathetically innervated tissues	Eskola et al.[a] (*40*)
^{68}Ga-EDTA	Renal function investigation	ICRP 80 (*49*)
^{68}Ga-DOTANOC	Tumors expressing somato-statin receptors	Pettinato et al. (*41*)

[a]The biokinetic data were extrapolated from the results of *ex vivo* studies in rats.

Supplemental Table 4. Weighting factors for calculation of effective dose of pregnant phantoms.

Organs	Weighting factors
Adrenals[b]	0.013
Bladder wall	0.04
Brain	0.01
Breasts	0.12
Esophagus	0.04
Gallbladder wall[b]	0.013
Heart wall[b]	0.013
Kidneys[b]	0.013
LI wall	0.12
Liver	0.04
Lungs	0.12
Ovaries	0.08
Pancreas[b]	0.013
SI wall and cont.	0.013
Skeleton[a]	0.13
Skin	0.01
Spleen[b]	0.013
Stomach wall	0.12
Thymus[b]	0.013
Thyroid	0.04
Uterine wall[b]	0.013
Remainder[b]	0.013

[a]Skeleton: bone marrow and bone surface.

[b]The tissue weights of adrenals, extrathoracic tissue, gall bladder, heart, kidneys, lymphatic nodes, muscle, oral mucosa, pancreas, small intestine (SI), spleen, thymus, uterus and salivary glands in ICRP103 were apportioned to adrenals, gallbladder wall, heart wall, kidneys, remainder, pancreas, SI wall and cont., spleen, thymus and uterine wall of the considered pregnant phantoms.
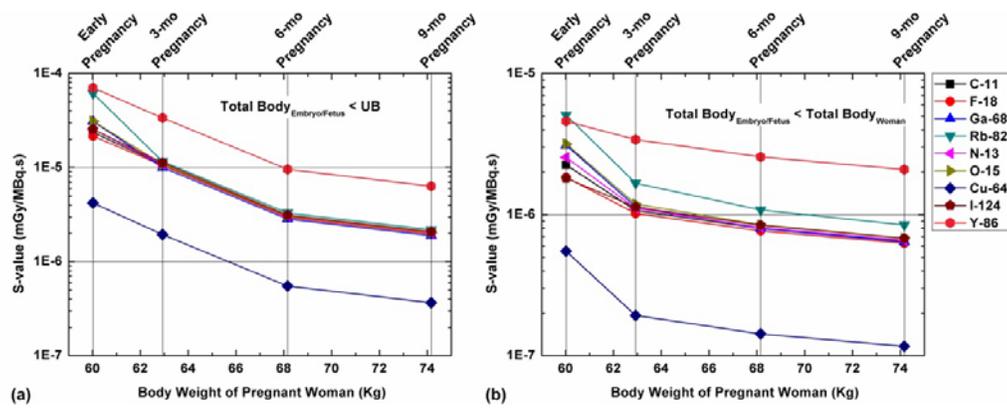
Supplemental Figure 1. Cross-absorbed S-values for (A) the UB irradiating the embryo/fetus and (B) the pregnant woman irradiating the embryo/fetus.
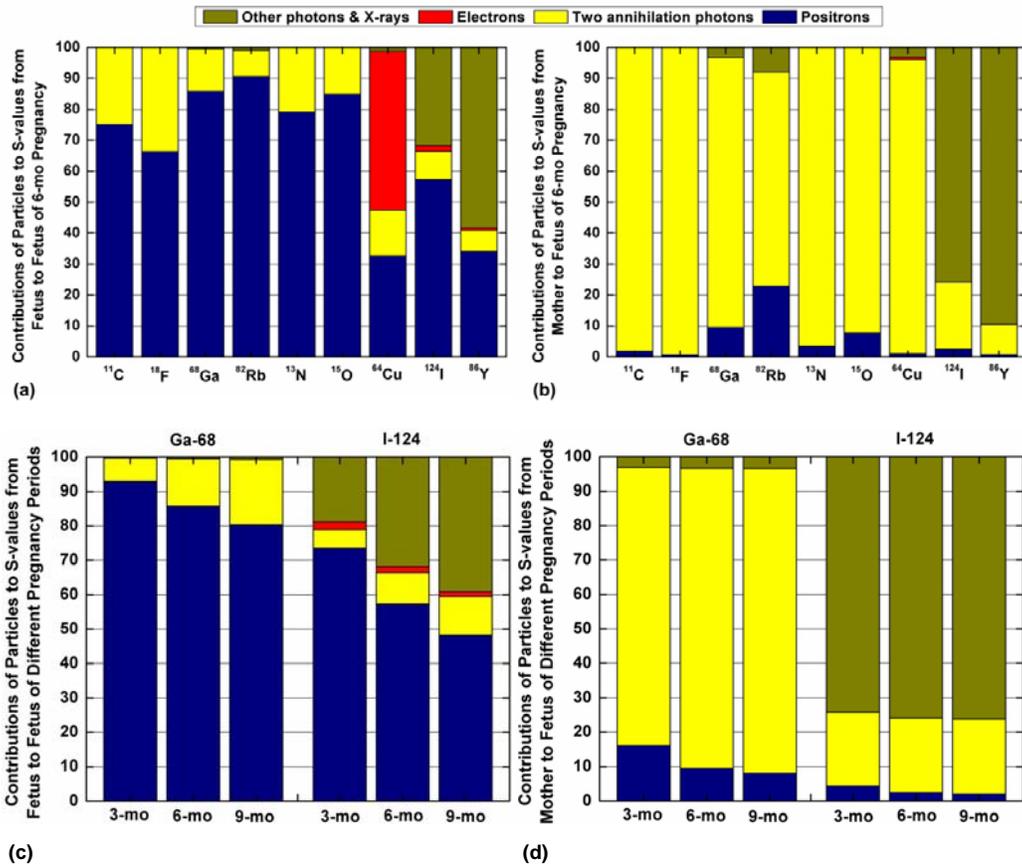
Supplemental Figure 2. Relative contributions of different types of radiation (positrons, annihilation photons, electrons, other photons and x-rays) to the estimated S-values of (A) fetus irradiating the fetus and (B) maternal body irradiating the fetus of the 6-mo pregnancy phantom for different radionuclides, and for Ga-68 and I-124 of (C) fetus irradiating the fetus and (D) maternal body irradiating the fetus of different pregnant phantoms.